ISSN 2347-3487

Evolution of unstable system.

Igor V. Lebed
Zhukovsky Central Institute of Aerohydrodynamics,
140180, Zhukovsky 3, Moscow, Russia,

Abstract

Scenario of appearance and development of instability in problem of a flow around a solid sphere at rest is discussed. The scenario was created by solutions to the multimoment hydrodynamics equations, which were applied to investigate the unstable phenomena. These solutions allow interpreting Stokes flow, periodic pulsations of the recirculating zone in the wake behind the sphere, the phenomenon of vortex shedding observed experimentally. In accordance with the scenario, system loses its stability when entropy outflow through surface confining the system cannot be compensated by entropy produced within the system. The system does not find a new stable position after losing its stability, that is, the system remains further unstable. As Reynolds number grows, one unstable flow regime is replaced by another. The replacement is governed tendency of the system to discover fastest path to depart from the state of statistical equilibrium. This striving, however, does not lead the system to disintegration. Periodically, reverse solutions to the multimoment hydrodynamics equations change the nature of evolution and guide the unstable system in a highly unlikely direction. In case of unstable system, unlikely path meets the direction of approaching the state of statistical equilibrium. Such behavior of the system contradicts the scenario created by solutions to the classic hydrodynamics equations. Unstable solutions to the classic hydrodynamics equations are not fairly prolonged along time to interpret experiment. Stable solutions satisfactorily reproduce all observed stable medium states. As Reynolds number grows one stable solution is replaced by another. They are, however, incapable of reproducing any of unstable regimes recorded experimentally. In particular, stable solutions to the classic hydrodynamics equations cannot put anything in correspondence to any of observed vortex shedding modes. In accordance with our interpretation, the reason for this is the classic hydrodynamics equations themselves.

Keywords

Instability, Multimoment Hydrodynamics, Entropy

Council for Innovative Research
Peer Review Research Publishing System
Journal: JOURNAL OF ADVANCES IN PHYSICS
Vol. 9, No. 3
www.cirjap.com, japeditor@gmail.com

ISSN 2347-3487

1. Introduction

Unstable processes are the fundamental manifestation of nature evolution. Vortex shedding behind a bluff bodies is the graphic example of an unstable process. A comparison of the results of direct numerical integration of the Navier–Stokes equations with the experimental data in unstable regime in problem on a flow around a solid sphere at rest revealed obvious discrepancies [1, 2].

Experiment records two stable stationary medium states represented by the $\mathbf{U}_0^{exp}(\mathbf{x})$ and $\mathbf{U}_1^{exp}(\mathbf{x})$ velocity distributions, and a stable non-stationary state of the central type with the $\mathbf{U}_2^{exp}(t,\mathbf{x})$ velocity distribution. Each of these three stable flows begins to develop in its own direction qualitatively different from other flows when it loses stability. The development occurs through a sequence of regular non-stationary periodic states schematically shown in Figure 1. Figure 1 was drawn on the basis of experimental data reviewed in [1]. Each of the three experimentally observed directions inevitably reaches periodic vortex shedding mode. Vortex shedding along each of the three directions is characterized by its own characteristic vortex shedding features intrinsic in it. However, irrespective of the direction selected experimentally, periodic vortex shedding is obligatory, well defined, and fairly prolonged along Reynolds numbers Re mode of the development of a turbulent process. Experiment records six vortex shedding modes, $\mathbf{W}_0^{exp}(t,\mathbf{x})$, $\mathbf{Q}_0^{exp}(t,\mathbf{x})$, $\mathbf{V}_1^{exp}(t,\mathbf{x})$, $\mathbf{V}_2^{exp}(t,\mathbf{x})$, $\mathbf{W}_2^{exp}(t,\mathbf{x})$ and $\mathbf{Q}_2^{exp}(t,\mathbf{x})$, and one pulsation mode $\mathbf{V}_0^{exp}(t,\mathbf{x})$. The recorded set of regular non-stationary periodic modes is most likely incomplete.

The direct numerical integration of the Navier–Stokes equations in problem on a flow around a solid sphere at rest was performed by various numerical methods. Nevertheless, the results of all these numerical experiments were absolutely identical (see review [1]). Calculations find two stationary stable solutions, $\mathbf{U}_0^{cal}(\mathbf{x})$ and $\mathbf{U}_1^{cal}(\mathbf{x})$ and a non-stationary stable solution of the central type, $\mathbf{U}_2^{cal}(t,\mathbf{x})$. Apart from these solutions, the Navier–Stokes equations only have a multiperiodic, that is, essentially chaotic, solution $\mathbf{U}_3^{cal}(t,\mathbf{x})$. According to calculations, the development of instability occurs in strict correspondence to the classic Landau–Hopf scenario [3]. After some critical Reynolds number value Re^{*} is reached, the ground axisymmetric stationary solution $\mathbf{U}_0^{cal}(\mathbf{x})$ loses its stability. Nonstationary solution $\mathbf{U}_{0,1}^{cal}(t,\mathbf{x},\mathrm{Re}^{*})$ ensures the transition from the $\mathbf{U}_0^{cal}(\mathbf{x})$ solution that lost its stability to the stable stationary nonaxisymmetric solution $\mathbf{U}_1^{cal}(\mathbf{x})$ (regular bifurcation). The attainment of the second critical Reynolds number value $\mathrm{Re}^{**} > \mathrm{Re}^{*}$ is accompanied by the loss of stability of the $\mathbf{U}_1^{cal}(\mathbf{x})$ solution. Nonstationary solution $\mathbf{U}_{1,2}^{cal}(t,\mathbf{x},\mathrm{Re}^{**})$ ensures the transition from the $\mathbf{U}_1^{cal}(\mathbf{x})$ solution that lost its stability to the stable nonstationary limiting cycle $\mathbf{U}_2^{cal}(t,\mathbf{x})$ (the Hopf bifurcation). After attainment of the third critical Reynolds number value $\mathrm{Re}^{***} > \mathrm{Re}^{**}$, the $\mathbf{U}_2^{cal}(t,\mathbf{x})$ solution loses its stability. Nonstationary solution $\mathbf{U}_{2,3}^{cal}(t,\mathbf{x},\mathrm{Re}^{***})$ ensures the transition from the $\mathbf{U}_2^{cal}(t,\mathbf{x})$ limiting cycle that lost its stability to the new stable position about which multiperiodic, that is, almost chaotic, $\mathbf{U}_3^{cal}(t,\mathbf{x})$ motion occurs. It follows that, according to the Landau–Hopf scenario, the system, after it loses stability, inevitably reaches a new stable position and exercises either periodic or chaotic motion about it. Calculations determine the direction of instability development, indicated by a dashed slant line in Figure 1.

The $\mathbf{U}_0^{cal}(\mathbf{x})$, $\mathbf{U}_1^{cal}(\mathbf{x})$, and $\mathbf{U}_2^{cal}(t,\mathbf{x})$ stable solutions satisfactorily reproduce $\mathbf{U}_0^{exp}(\mathbf{x})$, $\mathbf{U}_1^{exp}(\mathbf{x})$, and $\mathbf{U}_2^{exp}(t,\mathbf{x})$ stable flows. However, calculations can not put anything in correspondence to seven of ten experimentally observed modes schematically shown in Figure 1.

An attempt at removing obvious discrepancies between calculations and experiment was made earlier (see review [1,2]). The $\mathbf{U}_2^{cal}(t,\mathbf{x})$ limiting cycle is likely the only possibility of establishing correlation between the observed vortex shedding from a sphere, $\mathbf{V}_2^{exp}(t,\mathbf{x})$, and calculations. Indeed, the solutions $\mathbf{U}_0^{cal}(\mathbf{x})$ and $\mathbf{U}_1^{cal}(\mathbf{x})$ are stationary. The $\mathbf{U}_3^{cal}(t,\mathbf{x})$ mode following after the $\mathbf{U}_2^{cal}(t,\mathbf{x})$ monoperiodic mode is multiperiodic, that is, chaotic in essence. Correlation of $\mathbf{U}_3^{cal}(t,\mathbf{x})$ with the observed strictly periodic vortex shedding modes is hardly possible. Non-stationary solutions $\mathbf{U}_{0,1}^{cal}(t,\mathbf{x},\mathrm{Re}^{*})$, $\mathbf{U}_{1,2}^{cal}(t,\mathbf{x},\mathrm{Re}^{**})$, and $\mathbf{U}_{2,3}^{cal}(t,\mathbf{x},\mathrm{Re}^{***})$ are aperiodic, and are limited in time. Non-stationary solutions exist only at a critical values of the Reynolds number. These solutions cannot be put in correspondence to observed periodic vortex shedding modes exceedingly prolonged along the Re scale.

ISSN 2347-3487

The idea of attracting the stable central type mode $\mathbf{U}_2^{cal}(t,\mathbf{x})$ for the interpretation of the vortex shedding encounters the following objections. First, according to calculations, the regular solution gives way to the chaotic mode already at Re ~ 500. Experiment, however, shows that the vortex shedding mode is exceedingly prolonged along the Re scale. For instance, in an experiment in which a sphere was drawn at a constant rate through unperturbed medium, vortex shedding was recorded over the whole Re range studied, up to 30000. That is, calculations predict the transition to chaos early on the Re scale, which contradicts experiment. Secondly, at a moderately high Re, the $\mathbf{U}_2^{cal}(t,\mathbf{x})$ solution should simultaneously correspond to several non-stationary modes. For instance, at some $\mathrm{Re} > \mathrm{Re}_0^{***}$ value, experiment records four different vortex shedding modes, $\mathbf{Q}_0^{exp}(t,\mathbf{x})$ on the lower branch, $\mathbf{V}_1^{exp}(t,\mathbf{x})$ on the middle branch, and $\mathbf{W}_2^{exp}(t,\mathbf{x})$, and $\mathbf{Q}_2^{exp}(t,\mathbf{x})$ on the upper branch (Figure 1). One solution, namely, $\mathbf{U}_2^{cal}(t,\mathbf{x})$, cannot however simultaneously (at some $\mathrm{Re} > \mathrm{Re}_0^{***}$) correspond to four qualitatively different vortex shedding modes. Lastly, only three of six modes, $\mathbf{W}_0^{exp}(t,\mathbf{x})$, $\mathbf{V}_1^{exp}(t,\mathbf{x})$, and $\mathbf{V}_2^{exp}(t,\mathbf{x})$ are monoperiodic, whereas the $\mathbf{Q}_0^{exp}(t,\mathbf{x})$, $\mathbf{W}_2^{exp}(t,\mathbf{x})$ and $\mathbf{Q}_2^{exp}(t,\mathbf{x})$ modes are two-periodic. Clearly, the monoperiodic solution can by no means be put in correspondence to two-periodic modes.

As expected, the idea did not give the desired result. The streamline flow pictures for every quarter of the period of oscillations in the $\mathbf{U}_2^{cal}(t,\mathbf{x})$ recirculating zone in the near wake behind a sphere after the passage of some critical value Re_2^* are given in [4]. In accordance with calculation [4], after the appearance at a surface of the sphere, the vortex structure moves toward the periphery of the recirculating zone, which is accompanied by its continuous dissipation. Lastly, it fully disappears at the periphery of the recirculating zone. Because of the absence of the detachment of the recirculating zone periphery, there is no vortex street in the far wake behind a sphere. The streakline flow pictures don't detect also the slightest indications of vortex shedding [4].

This picture is qualitatively different from the observed full period of oscillation of the recirculating zone at supercritical values $\mathrm{Re} > \mathrm{Re}_2^*$ (see review [1]). As in calculations, the experimental vortex structure engendered begins to expand and move downstream within the near wake. After reaching the periphery of the recirculating zone, this vortex structure, however, acquires a maximum size rather than dissipates as predicted by calculations. At the end of the period, the vortex localized at the periphery of the recirculating zone separates from the core of recirculating zone. The separated vortex structure rushes downstream and forms a vortex street $\mathbf{V}_2^{exp}(t,\mathbf{x})$.

So, the $\mathbf{U}_2^{cal}(t,\mathbf{x})$ limiting cycle satisfactorily reproduced the $\mathbf{U}_2^{exp}(t,\mathbf{x})$ central type position at subcritical values $\mathrm{Re} < \mathrm{Re}_2^*$, but attempts to reproduce vortex shedding $\mathbf{V}_2^{exp}(t,\mathbf{x})$ at $\mathrm{Re} > \mathrm{Re}_2^*$ were a complete failure. In accordance with interpretation [1,2], stable solutions to Navier-Stokes equations successfully reach the boundary of instability field, indicated by a dashed slant line in Figure 1. As Re grows, these solutions move along this boundary. However, classic solutions are unable to cross the boundary and enter the instability field.

Most likely, the reason for this is Navier-Stokes equations themselves. Classic hydrodynamics equations exist for about two centuries. By definition, these equations are valid for the description of arbitrary continuous media corresponding to continuity and unlimited deformability principles [5]. Statistically grounded hydrodynamics equations are, however, far from being completely established. The greatest progress in this direction was made for one of continuous medium states, namely, for the rarefied gas state, where the characteristic free path λ far exceeded the characteristic size of particles d. In a rarefied gas, that is, at $d << \lambda$, the path from Newton equations written separately for each medium particle to classic hydrodynamics equations was passed without additional assumptions. The only exception was the Boltzmann hypothesis of molecular chaos "Stosszahlansatz" [6]. The Boltzmann hypothesis closes kinetic equation. An important result of statistical treatment was the conclusion that classic hydrodynamics equations derived heuristically were approximate. Indeed, classic hydrodynamics equations that directly follow from the Boltzmann equation inevitably contain the error involved in the derivation of classic kinetic equation. The physical meaning of this error, however, remains unclear. The physical meaning of the Boltzmann hypothesis was discovered in [7,2]. It was found that just the Boltzmann hypothesis, which closed Boltzmann kinetic equation, allowed us to construct hydrodynamics on only three lower principal hydrodynamic values. Binary collisions of particles tune the distributions of all the other hydrodynamic values to the distribution of three principal hydrodynamic values, $n(t,\mathbf{x})$, $\mathbf{U}(t,\mathbf{x})$, and $p(t,\mathbf{x})$. Here, $n(t,\mathbf{x})$ denotes the densities of the number of particles, $\mathbf{U}(t,\mathbf{x})$ is the hydrodynamic velocity, $p(t,\mathbf{x})$ is the pressure, $T(t,\mathbf{x})$ is the temperature, $p = nkT$, k is the Boltzmann constant That is, all the higher hydrodynamic values become functions of only three principal hydrodynamic values. In particular, the viscous stress tensor $p_{ij}(t,\mathbf{x})$ becomes directly proportional to the deformation tensor of velocities (the Newton law), and the heat flux vector $\mathbf{q}(t,\mathbf{x})$ becomes directly proportional to the gradient of temperature (the Fourier law). Since the classic

three-moment hydrodynamics is constructed without the use of higher principal hydrodynamic values, its applicability range is limited to states that are only weakly removed from the statistical equilibrium state.

Analysis [8] substantiates the suggestion that the applicability range of three-moment classic hydrodynamics equations is limited, in particular, by small Reynolds number values $\mathrm{Re} << 1$. Nevertheless, the calculated stable solutions to Navier–Stokes equations, namely, $\mathbf{U}_0^{cal}(\mathbf{x})$, $\mathbf{U}_1^{cal}(\mathbf{x})$, and $\mathbf{U}_2^{cal}(t,\mathbf{x})$, satisfactorily reproduced stable flows $\mathbf{U}_0^{exp}(\mathbf{x})$, $\mathbf{U}_1^{exp}(\mathbf{x})$, and $\mathbf{U}_2^{exp}(t,\mathbf{x})$ recorded experimentally at moderately high Reynolds number values, which reached several hundreds. This means that the error contained in solutions to the Navier–Stokes equations is not too large, that is, it does not introduce visually observable changes into the picture of stable flows. This error, however, begins to increase sharply after the critical Reynolds number value accompanied by stability loss is exceeded. An increase in error is caused by the ability of nonlinear equations to exponentially quickly separate initially close solutions even in a limited phase space region. This sensitivity to initial conditions was called the Lorentz butterfly effect [3]. Loss of the direction of instability development is a result of an increase in the error. That is, classic hydrodynamics equations are absolutely incapable of reproducing unstable periodic flows, which appear after the critical Reynolds number is exceeded.

The present study is devoted to the discussion of the contribution of entropy in determining the direction of system evolution after stability loss. Section 1 presents the stability principle and the evolution criterion. Section 2 presents the results of numerical integration of the multimoment hydrodynamics equations in the problem of a flow around a solid sphere. The stability principle elucidates the cause of stability loss after attainment of the first critical Reynolds number. The evolution criterion elucidates the cause of appearance of the vortex shedding after attainment of the next critical Reynolds number.

2. Stability principle and evolution criterion.

The possibility of the improvement of classic hydrodynamics equations should be sought by increasing the number of principal hydrodynamic values. “The passage to hydrodynamics” from 12-dimensional space of two particles was found in [9,7]. The formalism of this method allows hydrodynamic equations to be derived with an arbitrary number of principal hydrodynamic values. Hydrodynamics formulated on the basis of pair distribution functions moments can appropriately be called multimoment hydrodynamics. In [7], multimoment hydrodynamics equations were constructed using seven principal hydrodynamic values. Just these seven principal hydrodynamic values are measurable moments and determined by the one-particle distribution function. In conformity with continuity and unlimited deformability principles [5], multimoment hydrodynamics equations [7] are suggested for use for any continuous medium state rather than for the rarefied gas state only.

Pair distribution functions $f_p^{app}(t,\mathbf{x},\mathbf{G},\mathbf{v})$ and $f_p^{div}(t,\mathbf{x},\mathbf{G},\mathbf{v})$ are specified in [9], where $\mathbf{G}$ is velocity of the center of mass of pair of particles, and $\mathbf{v}$ is relative velocity of pair of particles. Heuristic derivation of a set of equations for pair distribution functions $f_p^{app}(t,\mathbf{x},\mathbf{G},\mathbf{v})$ and $f_p^{div}(t,\mathbf{x},\mathbf{G},\mathbf{v})$ was given in [10]. In [9,11], equations for pair distribution functions were derived directly from the fundamental statistical mechanics concepts. Functions $f_p^{app}(t,\mathbf{x},\mathbf{G},\mathbf{v})$ and $f_p^{div}(t,\mathbf{x},\mathbf{G},\mathbf{v})$ evolve with progressive direction of timing along the time axis pointing from the past to the future.

The lower moments of the pair distribution functions are the local density of the number of pairs $n^G(t,\mathbf{x})$, the mean velocity of the centers of mass of pairs $\mathbf{U}^G(t,\mathbf{x})$, the $P_{ij}^G(t,\mathbf{x})$ tensor of stresses created as a result of movement of the centers of mass of pairs of particles, the $P_{ij}^v(t,\mathbf{x})$ tensor of stresses created because of relative movement of pair particles, the $\mathbf{q}^G(t,\mathbf{x})$ heat flux vector corresponding to the transfer of thermal energy because of movement of the centers of mass of pairs of particles, $\mathbf{q}^v(t,\mathbf{x})$ and $\mathbf{q}^{Gv}(t,\mathbf{x})$ the and heat flux vectors corresponding to thermal energy transfer because of relative movement of particles in pairs. Along with $P_{ij}^G(t,\mathbf{x})$ and $P_{ij}^v(t,\mathbf{x})$ let us determine small stress tensors $p_{ij}^G(t,\mathbf{x})$ and $p_{ij}^v(t,\mathbf{x})$, and $p^G(t,\mathbf{x})$ and $p^v(t,\mathbf{x})$ pressure, and $T^G(t,\mathbf{x})$ and $T^v(t,\mathbf{x})$ temperature, $p^G = n^G kT^G$, $p^v = n^G kT^v$. The lower moments of the pair distribution functions are determined in [7]. The set of seven hydrodynamic values, namely, $n^G(t,\mathbf{x})$, $\mathbf{U}^G(t,\mathbf{x})$, $p^G(t,\mathbf{x})$, $p^v(t,\mathbf{x})$, $p_{ij}^G(t,\mathbf{x})$, $\mathbf{q}^G(t,\mathbf{x})$, and $\mathbf{q}^v(t,\mathbf{x})$, is a set of the principal hydrodynamic values. The lower moments $p_{ij}^v(t,\mathbf{x})$ and $\mathbf{q}^{Gv}(t,\mathbf{x})$ are the non-principal hydrodynamic values.

The relations between the one-particle distribution function and the pair distribution functions [7] can be used to find a relation between the one-particle distribution function and the pair distribution functions moments,

$$n = n^G \qquad \mathbf{U} = \mathbf{U}^G \qquad p = \frac{1}{2}p^G + \frac{1}{2}p^v \qquad T = \frac{1}{2}T^G + \frac{1}{2}T^v \qquad (2.1)$$

$$P_{ij} = \frac{1}{2}P_{ij}^G + \frac{1}{2}P_{ij}^v \qquad p_{ij} = \frac{1}{2}p_{ij}^G + \frac{1}{2}p_{ij}^v \qquad \mathbf{q} = \frac{1}{2}\mathbf{q}^G + \frac{5}{6}\mathbf{q}^v + \mathbf{q}^{Gv}$$

Derivation of conservation equations determining seven moments of the pair distribution functions is given in [7]. Expressions for non-principal hydrodynamic values are represented in [7] also. In [12,13], this set of multimoment hydrodynamics equations is reduced to a closed set of nonlinear differential equations of the *n*th order for dimensionless coefficients $\hat{C}_i(t)$:

$$\frac{\partial \hat{C}_i}{\partial t} = F_i(\hat{C}_1,...,\hat{C}_n) \qquad i = 1,...,n \qquad (2.2)$$

Let $\hat{\bar{C}}_i^{(\alpha)}$ be a stationary α-solution to the set (2.2), $\delta\hat{C}_i^{(\alpha)}(t)$ is a fluctuation of the solution $\hat{\bar{C}}_i^{(\alpha)}$, and $\hat{C}_i^{(\alpha)}(t) = \hat{\bar{C}}_i^{(\alpha)} + \delta\hat{C}_i^{(\alpha)}(t)$. The coefficients $\hat{C}_i^{(\alpha)}(t)$ make it possible to calculate the distributions of the hydrodynamic values (2.1).

Superscript * marks the pair distribution functions $f_p^{*app}(t^*,\mathbf{x},\mathbf{G},\mathbf{v})$ and $f_p^{*div}(t^*,\mathbf{x},\mathbf{G},\mathbf{v})$, which evolve with progressive direction of timing along the time axis pointing from the future to the past. The set of reverse equations for pair distribution functions $f_p^{*app}(t^*,\mathbf{x},\mathbf{G},\mathbf{v})$ and $f_p^{*div}(t^*,\mathbf{x},\mathbf{G},\mathbf{v})$ was derived in [8,14].

Reverse multimoment hydrodynamics equations can be derived from equations for pair distribution functions $f_p^{*app}(t^*,\mathbf{x},\mathbf{G},\mathbf{v})$ and $f_p^{*div}(t^*,\mathbf{x},\mathbf{G},\mathbf{v})$ within the formalism of [7]. It turned out that the form of the resulting equations of conservation is invariant with respect to the direction of the time axis. Principal hydrodynamic values, namely, $n^*(t^*,\mathbf{x})$, $\mathbf{U}^*(t^*,\mathbf{x})$, $p^{*G}(t^*,\mathbf{x})$, $p^{*v}(t^*,\mathbf{x})$, $p_{ij}^{*G}(t^*,\mathbf{x})$, $\mathbf{q}^{*G}(t^*,\mathbf{x})$, and $\mathbf{q}^{*v}(t^*,\mathbf{x})$, are the moments of the reverse pair function $f_p^{*app}(t^*,\mathbf{x},\mathbf{G},\mathbf{v})$ and $f_p^{*div}(t^*,\mathbf{x},\mathbf{G},\mathbf{v})$. Expressions for the reverse moments are identical to expressions for the moments of the direct pair functions $f_p^{app}(t,\mathbf{x},\mathbf{G},\mathbf{v})$ and $f_p^{div}(t,\mathbf{x},\mathbf{G},\mathbf{v})$ presented in [7]. However, expressions for the non-principal hydrodynamic values from [7] undergo transformations. Namely, the reverse multimoment hydrodynamics equations give the expressions for the stress tensor $p_{ij}^{*v}(t^*,\mathbf{x})$ and heat flux vector $\mathbf{q}^{*Gv}(t^*,\mathbf{x})$ differ from their counterparts stemming from the direct multimoment hydrodynamics equations by their sign [8,14].

In [12], the reverse multimoment hydrodynamics equations are reduced to a closed set of nonlinear differential equations of the *n*th order for dimensionless coefficients $\hat{C}_i^*(t)$:

$$\frac{\partial \hat{C}_i^*}{\partial t^*} = F_i(\hat{C}_1^*,...,\hat{C}_n^*) \qquad i = 1,...,n \qquad (2.3)$$

Let $\hat{C}_i^{*(\alpha)}(t^*) = \hat{\bar{C}}_i^{*(\alpha)} + \delta\hat{C}_i^{*(\alpha)}(t^*)$ be α-solution to the set (2.3).

Superscript $^+$ marks the pair distribution functions $f_p^{+app}(t^+,\mathbf{x},\mathbf{G},\mathbf{v})$ and $f_p^{+div}(t^+,\mathbf{x},\mathbf{G},\mathbf{v})$, which evolve with regressive direction of timing along the time axis pointing from the past to the future. In [8,14], we failed to derive a set of equations for pair distribution functions $f_p^{+app}(t^+,\mathbf{x},\mathbf{G},\mathbf{v})$ and $f_p^{+app}(t^+,\mathbf{x},\mathbf{G},\mathbf{v})$. However, solutions to the reverse equations for pair distribution functions $f_p^{*app}(t^*,\mathbf{x},\mathbf{G},\mathbf{v})$ and $f_p^{*div}(t^*,\mathbf{x},\mathbf{G},\mathbf{v})$, and reverse multimoment hydrodynamics equations they yield are also applicable to interpret observed system evolution with regressive timing along the time axis pointing from the past to the future.

Local pair entropy $\bar{S}_p(t,\mathbf{x})$ is specified in [13]. The $\bar{S}_p(t,\mathbf{x})$ entropy is defined in terms of pair distribution function labeled by *app* superscript:

ISSN 2347-3487

$$\bar{S}_p(t,\mathbf{x}) = -k\int f_p^{app}(t,\mathbf{x},\mathbf{G},\mathbf{v})\ln f_p^{app}(t,\mathbf{x},\mathbf{G},\mathbf{v})d\mathbf{G}d\mathbf{v} \quad \bar{S}_p(t) = \int \bar{S}_p(t,\mathbf{x})d\mathbf{x} \qquad (2.4)$$

In [13], when deriving equations of entropy conservation, we reasoned from the concept of a Gibbs ensemble of systems. When modeling an individual system, each hydrodynamic value in the equations of conservation should be supplemented with its fluctuation component [15]:

$$\frac{\partial S_p^{(\alpha)}(t)}{\partial t} + \Delta_{\text{EX}} S_p^{(\alpha)}(t) = \Delta_{\text{IN}} S_p^{(\alpha)}(t) \qquad S_p^{(\alpha)}(t) = \bar{S}_p^{(\alpha)}(t) + \delta S_p^{(\alpha)}(t) \qquad (2.5)$$

The $\bar{S}_p^{(\alpha)}(t)$ function characterizes the ensemble of systems as a whole. The $\delta S_p^{(\alpha)}(t)$ function is fluctuation of the $\bar{S}_p^{(\alpha)}(t)$ pair entropy. Here, superscript (α) corresponds to the α-solution to the multimoment hydrodynamics equations (2.2). In accordance with (2.5), evolution of the $S_p^{(\alpha)}(t)$ pair entropy is defined by two factors, by the $\Delta_{\text{IN}} S_p^{(\alpha)}(t)$ entropy production in the system and the $\Delta_{\text{EX}} S_p^{(\alpha)}(t)$ entropy outflow through the surface confining the system. The $S_p^{(\alpha)}(t)$ entropy conveys the meaning of volume occupied by the system in the Γ-space [13]. The study undertaken in [13] has revealed that the local pair entropy can only be produced in the system due to binary collisions at any space point $\mathbf{x}$ and at any instant t, $\Delta_{\text{IN}} S_p^{(\alpha)}(t,\mathbf{x}) \geq 0$. Thus, at any instant binary collisions merely rise the pair entropy of the system, $\Delta_{\text{IN}} S_p^{(\alpha)}(t) \geq 0$.

Let us restrict consideration exclusively to entropy fluctuations with $\delta S_p^{(\alpha)}(t) < 0$. The reason for this "asymmetry" is considered in [13]. The principle according to which an open system retains (or loses) its stability is formulated as follows.

An open system with time-independent boundary conditions has a stable stationary $\alpha-$state with entropy $\bar{S}_p^{(\alpha)}$ while entropy production in it exceeds entropy outflow through the surface confining the system for $\delta S_p^{(\alpha)}(t) \leq 0$

$$[\Delta_{\text{IN}} S_p^{(\alpha)}(t) - \Delta_{\text{EX}} S_p^{(\alpha)}(t)] \geq 0, \quad t \geq 0, \quad for \quad \delta S_p^{(\alpha)}(t) \leq 0 \qquad (2.6)$$

As soon as the parameters characterizing the system reach the values, at which inequality (2.6) fails, the stationary $\alpha-$state of the open system becomes unstable.

The principle originally formulated for open system with time-independent boundary conditions can be expected to the case of open systems with time-dependent boundary conditions. Generally, entropy $\bar{S}_p^{(\alpha)}(t)$ corresponding to an ensemble of systems may not be reckoned as stationary value. That is why, generally, the stability principle is formulated in terms of excess of the entropy production $\Delta_{\text{IN}} \delta S_p^{(\alpha)}(t)$ and excess of the entropy outflow $\Delta_{\text{EX}} \delta S_p^{(\alpha)}(t)$.

The $\alpha-$state with entropy $\bar{S}_p^{(\alpha)}(t)$ of an open system remains stable while the excess of entropy production generated in the system exceeds its excess of outflow through the surface confining the system for $\delta S_p^{(\alpha)}(t) \leq 0$

$$[\Delta_{\text{IN}} \delta S_p^{(\alpha)}(t) - \Delta_{\text{EX}} \delta S_p^{(\alpha)}(t)] \geq 0, \quad t > 0, \quad for \quad \delta S_p^{(\alpha)}(t) \leq 0 \qquad (2.7)$$

As soon as the parameters characterizing the system reach the values, at which inequality* (2.7) *fails, the $\alpha-$state of the open system becomes unstable.

Inequality (2.6) for systems with time-independent boundary conditions is reduced to inequality (2.7). However, the stability principle for stationary states (2.6) seems to be more "transparent".

In accordance with the principle of retention and loss of stability (2.7), in an open unstable system, any entropy fluctuation $\delta S_p^{(\alpha)}(t=0) < 0$ begins to grow. In particular, for a system with time-independent boundary conditions

ISSN 2347-3487

$$\frac{\partial \delta S_p^{(\alpha)}(t)}{\partial t} = \frac{\partial S_p^{(\alpha)}(t)}{\partial t} < 0 \quad for \quad \delta S_p^{(\alpha)}(t=0) < 0 \qquad (2.8)$$

Based on the expression (2.8), we formulated the criterion of evolution of an open system with lost stability [16,17]:

An open unstable system with time-independent boundary conditions, takes a direction of evolution that provides the most rapid decrease in entropy.

Namely, of the two directions of development of the instability, having the same values of the entropy at the time $t = t_0$, fluctuations find such a direction that is characterized by lower value of the derivative of entropy:

$$\left.\frac{\partial S_p^{(\alpha)}(t)}{\partial t}\right|_{t=t_0} < \left.\frac{\partial S_p^{(\beta)}(t)}{\partial t}\right|_{t=t_0} \qquad (2.9)$$

wherein

$$\left. S_p^{(\alpha)}(t)\right|_{t=t_0} = \left. S_p^{(\beta)}(t)\right|_{t=t_0}$$

$$for \quad \delta S_p^{(\alpha)}(t=0) < 0 \qquad \delta S_p^{(\beta)}(t=0) < 0$$

That is, at the time $t = t_0 > 0$, the system takes the α-direction, for which the derivative of the entropy with respect to time has a lower value compared to the respectively derivative for the β-direction.

Let us consider the case of equality of derivatives. Then, of the two directions of development of the instability, having the same values of the entropy and entropy derivative at the time $t = t_0$, fluctuations find such a direction that is characterized by lower value of the second derivative of entropy:

$$\left.\frac{\partial^2 S_p^{(\alpha)}(t)}{\partial t^2}\right|_{t=t_0} < \left.\frac{\partial^2 S_p^{(\beta)}(t)}{\partial t^2}\right|_{t=t_0} \qquad (2.10)$$

wherein

$$\left. S_p^{(\alpha)}(t)\right|_{t=t_0} = \left. S_p^{(\beta)}(t)\right|_{t=t_0}, \quad \left.\frac{\partial S_p^{(\alpha)}(t)}{\partial t}\right|_{t=t_0} = \left.\frac{\partial S_p^{(\beta)}(t)}{\partial t}\right|_{t=t_0}$$

$$for \quad \delta S_p^{(\alpha)}(t=0) < 0 \qquad \delta S_p^{(\beta)}(t=0) < 0$$

That is, at the time $t = t_0 > 0$, the system takes the α-direction, for which the second derivative of the entropy with respect to time has a lower value compared to the respectively derivative for the β-direction.

Local pair entropy $\bar{S}_p^*(t^*, \mathbf{x})$ is defined in terms of pair distribution function labeled by *div* superscript:

$$\bar{S}_p^*(t^*, \mathbf{x}) = -k \int f_p^{*div}(t^*, \mathbf{x}, \mathbf{G}, \mathbf{v}) \ln f_p^{*div}(t^*, \mathbf{x}, \mathbf{G}, \mathbf{v}) d\mathbf{G} d\mathbf{v} \qquad \bar{S}_p^*(t^*) = \int \bar{S}_p^*(t^*, \mathbf{x}) d\mathbf{x} \qquad (2.11)$$

The equation of entropy conservation assumes the form:

$$\frac{\partial S_p^{*(\alpha)}(t^*)}{\partial t^*} + \Delta_{EX} S_p^{*(\alpha)}(t^*) = \Delta_{IN} S_p^{*(\alpha)}(t^*) \qquad S_p^{*(\alpha)}(t^*) = \bar{S}_p^{*(\alpha)}(t^*) + \delta S_p^{*(\alpha)}(t^*) \qquad (2.12)$$

The study undertaken in [13] has revealed that the local pair entropy can only be absorbed in the system due to binary collisions at any space point $\mathbf{x}$ and at any instant t^*, $\Delta_{\mathrm{IN}} S_p^{*(\alpha)}(t^*, \mathbf{x}) \le 0$. Thus, at any instant binary collisions absorb the pair entropy of the system, $\Delta_{\mathrm{IN}} S_p^{*(\alpha)}(t^*) \le 0$.

3. Entropy interpretation of appearance and development of instability.

In [12,13,16,17], the multimoment hydrodynamics equations are used to study the phenomena of instability appearance and development in problem on flow around a solid sphere at a wide range of Reynolds number values. The study [12,16] demonstrated that at small Re the simplest solution to the multimoment hydrodynamics equations coincides with the Stokes solution to the classic hydrodynamics equations. Further, in [12,16], the closed set of nonlinear differential equations (2.2) was reduced to a set of 20th order, S20. Numerical integration of this set has revealed stable root $\hat{C}_i = \hat{\bar{C}}_i^{(0)}$, *i* = 1, …, 20. According to the stationary solution $\hat{\bar{C}}_i^{(0)}$, *i* = 1, …, 20, an axisymmetric recirculating zone is formed in the wake behind the sphere at Re ~20. It expands as Re grows but its shape remains unchanged. The stationary solution $\hat{\bar{C}}_i^{(0)}$, *i* = 1, …, 20, remains stable up to a certain critical value of $\mathrm{Re}_0^* = 129.1$.

Values of the dimensionless pair entropy derivative calculated from the solution $\hat{\bar{C}}_i^{(0)}$, *i* = 1, …, 20, at Re close to Re_0^* are plotted at Figure 2. The pair entropy is calculated in the dominant order, $S_p^{(0)}(t) = k n_0 v_0 \mathrm{Ma}^4 \hat{S}_p^{(0)}(t)$, where $\mathrm{v}_0 = (4/3)\pi a^3$, $\mathrm{Ma}^2 = m U_0^2 / k T_0$, m is the mass of the particle, T_0 and n_0 are the temperature and the density of the unperturbed medium, U_0 is the incoming flow velocity. The characteristic time scale of the problem is $a\,\mathrm{Re}/2U_0$, whereas the characteristic spatial scale is the radius of the sphere a. The Reynolds number is calculated from the diameter of the sphere: $\mathrm{Re} = 2 m n_0 U_0 a / \eta_0$, where $\eta_0 = \eta(T_0)$ is the dynamic viscosity. The details of the calculation are represented in [13].

As revealed by calculations [13], $\partial \delta S_p^{(0)}(t) / \partial t\big|_{t=0} > 0$ at $\mathrm{Re} < \mathrm{Re}_0^*$. In this case, in accordance with (2.5), entropy production in the system exceeds the entropy outflow through the surface confining the system. Then, in accordance with the principle of retention and loss of the open system stability (2.6), the stationary $\hat{\bar{C}}_i^{(0)}$, *i* = 1, …, 20, solution remains stable. Pair entropy derivative $\partial \delta S_p^{(0)}(t) / \partial t\big|_{t=0} < 0$ at $\mathrm{Re} > \mathrm{Re}_0^*$. That is, after the passage of Re_0^*, in accordance with (2.5), entropy outflow through the surface confining the system begins to exceed the entropy production in the system. Then, in accordance with the principle of retention and loss of the open system stability (2.6), the stationary $\hat{\bar{C}}_i^{(0)}$, *i* = 1, …, 20, solution becomes unstable.

This means that, at $\mathrm{Re} > \mathrm{Re}_0^*$, starting from the time $t = 0$, small axisymmetric fluctuations $\delta \hat{C}_i^{(0)}(t) < 0$ of the solutions $\hat{\bar{C}}_i^{(0)}$, *i* = 1, …, 20, begin to grow exponentially. The fluctuations grow up until a time $t = t_* > 0$. At the time $t = t_*$, the solution $\hat{C}_i^{(0)}(t)$ breaks down. Why the solution terminates at $t = t_*$ is explained in [12].

It turns out that, in the vicinity of the breakdown point, there exists a solution $\hat{C}_i^{*(0)}(t^*)$, *i* = 1, …, 20, to the closed set (2.3) of 20th order, S^*20. At the time $t = t_*$, the solutions $\hat{\bar{C}}_i^{(0)}$ is replaced by the solution $\hat{C}_i^{*(0)}$. Further, it appears that, by the time $t = 2t_*$, the solution $\hat{C}_i^{*(0)}(t^*)$ reaches the neighborhood of the stationary solution $\hat{\bar{C}}_i^{(0)}$, *i* = 1, …, 20. The solution $\hat{\bar{C}}_i^{(0)}$ is unstable. Thus, starting from the time $t = 2t_*$, small axisymmetric fluctuations $\delta \hat{C}_i^{(0)}(t) < 0$ grow. This process is repeated periodically [12]. The solution $\hat{C}_i^{(0)}(t)$ exists within $0 \le t \le t_*$. The solution $\hat{C}_i^{*(0)}(t^*)$ exists in the range $t_* \le t \le 2t_*$. Time t is reckoned in progressive direction along the time axis pointing from the past to the future.

Time t^* is reckoned in progressive direction along the time axis pointing from the future to the past. Let us agree upon the origin and put $t^* = t_*$ for the moment of time $t = t_*$.

Designate the solution $\hat{C}_i^{(0)}(t)$, $\hat{C}_i^{*(0)}(t^*)$, *i* = 1, …, 20, as Sol_0. According to the Sol_0 solution, after the attainment of $\mathrm{Re} = \mathrm{Re}_0^*$, the periphery of the recirculating zone begins to pulsate periodically. Pulsating periphery demonstrates the absence of slightest indications of detachment from the core of the recirculating zone. As a consequence, there is no vortex street in the far wake behind a sphere. So, the Sol_0 solution does not describe a vortex shedding.

The studies [16,17] are devoted to finding solutions to the multimoment hydrodynamics equations, which enable to interpret the phenomenon of vortex shedding. In [16,17], we obtain a closed set of nonlinear equations of the twenty-second order S22 for the coefficients $\hat{C}_i(t)$, $i = 1,...,22$. It turned out that, in the investigated range of Re, of great many solutions to the set S22, only two solutions correspond to such an pair entropy value that allows these solutions to compete with the solution Sol_0. We denote the solution $\hat{C}_i^{(1)}(t)$, $i = 1,...,22$, as Sol_1, and the solution $\hat{C}_i^{(2)}(t)$, $i = 1,...,22$, as Sol_2. Both the Sol_1 solution and the Sol_2 solution describe a vortex ring behind the sphere moving downstream.

Figure 3 shows the time dependence of the dimensionless pair entropy $S_p^{(0)}(t)$ calculated from the Sol_0 solution at Re = 400. The details of the calculation are represented in [16,17]. Beginning from the time $t = 0$ up to the time $t = t_*$, the entropy decreases permanently. This behavior of the entropy corresponds to the receding of the state of a system that lost stability from the state of statistical equilibrium. At the time $t = t_*$, the Sol_0 solution to the multimoment hydrodynamics equations breaks down. The movement of the representative point over the curve (Figure 3) from $t = t_*$ to $t = 2t_*$ corresponds to the return of the recirculating zone to its original position, i.e., the position corresponding to the time $t = 0$. Since the time $t = t_*$, the movement of the representative point is described by the reverse multimoment hydrodynamics equations. The reverse set of equations (2.3) is solved with progressive timing along the time axis. The positive direction of this time axis runs from the future to the past. However, the solutions to the reverse set of equations (2.3) may be used to interpret evolution with regressive direction of timing along the time axis pointing from the past to the future (Figure 3):

$$\hat{C}_i^{*(0)}(t^*) = \hat{C}_i^{+(0)}(t^+) \qquad (3.1)$$

The solution $\hat{C}_i^{*(0)}(t^*)$ exists in the range $t_* \le t^* \le 2t_*$. The connection between times on the different time axes is $t^+ = -t^* + 2t_*$. The distribution of the hydrodynamics values (2.1) involved in the expressions for $S_p^{(0)}(t)$ and $S_p^{*(0)}(t^*)$ are conjugated with the coefficients $\hat{C}_i^{(0)}(t)$ and $\hat{C}_i^{*(0)}(t^*)$ $i = 1,...,20$ [16], then,

$$S_p^{*(0)}(t^*) = S_p^{+(0)}(t^+) \qquad \frac{\partial S_p^{*(0)}(t^*)}{\partial t^*} = -\frac{\partial S_p^{+(0)}(t^+)}{\partial t^+} \qquad (3.2)$$

The regressive timing order along the time axis pointing from the past to the future is represented on the axis beneath the abscissa in Figure 3 ($t^+ = -t + 2t_*$ within $t_* \le t \le 2t_*$). The $S_p^{(0)}(t)$ pair entropy exists in the range $0 \le t \le t_*$, whereas the $S_p^{+(0)}(t^+)$ pair entropy, within $0 \le t^+ \le t_*$, or $t_* \le t \le 2t_*$.

In accordance with symmetry properties of solutions to sets (2.2) and (2.3) [12,16], at any moment of time $t = t_0$ within $0 \le t_0 \le t_*$, there exist the relationships:

$$\hat{C}_i^{(0)}(t)\Big|_{t=t_0} = \hat{C}_i^{*(0)}(t^*)\Big|_{t^*=2t_*-t_0} = \hat{C}_i^{+(0)}(t^+)\Big|_{t^+=t_0} \qquad (3.3)$$

ISSN 2347-3487

Relationships (3.3) between the coefficients $\hat{C}_i^{+(0)}(t^+)$, $\hat{C}_i^{*(0)}(t^*)$, and $\hat{C}_i^{(0)}(t)$ for any moment of time t_0 within $0 \le t_0 \le t_*$ give:

$$S_p^{(0)}(t)\Big|_{t=t_0} = S_p^{*(0)}(t^*)\Big|_{t^*=2t_*-t_0} = S_p^{+(0)}(t^+)\Big|_{t^+=t_0}$$

$$\frac{\partial S_p^{(0)}(t)}{\partial t}\Big|_{t=t_0} = -\frac{\partial S_p^{*(0)}(t^*)}{\partial t^*}\Big|_{t^*=2t_*-t_0} = \frac{\partial S_p^{+(0)}(t^+)}{\partial t^+}\Big|_{t^+=t_0} \qquad (3.4)$$

Function $\tilde{S}_p^{(0)}(t-t^{(0)})$ is a portion of the pair entropy $S_p^{(0)}(t)$, which specifies the behavior of the entropy in the neighborhood $t_* - t^{(0)}$ of the point of solution breakdown, $t = t_*$:

$$S_p^{(0)}(t) = \tilde{S}_p^{(0)}(t-t^{(0)}) \qquad (3.5)$$

The curve 1 in Figure 4 specifies the time behavior of the pair entropy derivative calculated from the solution Sol_0, which describes recirculating zone in the wake behind a sphere. The details of the calculation are represented in [16,17]. The curve 2 in Figure 4 specifies the combination of the solutions Sol_0 and Sol_1. In this combination the Sol_0 solution describes the core of the recirculating zone in the near wake and the Sol_1 solution describes the periphery of the recirculating zone and the far wake. Curves 1 and 2 intersect at a restructuring time of $t = t_1$. After the attainment of the time $t = t_1$, the Sol_0 solution is replaced by the combination of the solutions Sol_0 and Sol_1. The reason for the replacement is that the combination of the solutions Sol_0 and Sol_1 becomes more preferable in comparison with the Sol_0 solution. The combination of the solutions Sol_0 and Sol_1 provides a sharper drop in the entropy in the course of evolution than the Sol_0 solution does. The criterion (2.10) dictates the choice of the direction of development that is given by combination of the solutions Sol_0 and Sol_1. The movement of the representative point over the curve 1 up to $t = t_1$ is not accompanied by rearrangement of the flow. The behavior of the flow at $t < t_1$ corresponds to the criterion (2.9). Starting from the restructuring time of $t = t_1$, the periphery of the recirculating zone separates from its core, moving downstream in the form of a vortex ring. This process is repeated periodically [16,17].

4. Results and discussion.

According to the experimental data, at $\mathrm{Re} \sim$ 10–20, a steady toroidal recirculating zone arises in the near wake behind the sphere formed $\mathbf{U}_0^{exp}(\mathbf{x})$, which increases in size with increasing Re. After reaching the first critical value of the Reynolds number Re_0^*, the recirculating zone periphery begins to pulsate periodically. During pulsations, the front side of the recirculating zone is strictly attached to the surface of the sphere. The pulsing flow $\mathbf{V}_0^{exp}(t,\mathbf{x})$ remains axisymmetric. With the growth of Re, pulsations become more pronounced, and their amplitude increases. After passing the second critical value of Re_0^{**}, the periphery of the recirculating zone begins periodically separate from its core, moving downstream in the form of a vortex ring. Vortex rings recede downstream from the sphere, keeping a noticeable distance from each other (the $\mathbf{W}_0^{exp}(t,\mathbf{x})$ mode). Achieving the third critical value of Re_0^{***} is accompanied by an instantaneous change in the mode of vortex shedding from the sphere. The frequency of vortex shedding increases, while the gaps between the vortex rings disappear. Vortex rings penetrate one another, forming a continuous vortex sheet $\mathbf{Q}_0^{exp}(t,\mathbf{x})$ in the wake behind the sphere.

ISSN 2347-3487

The stationary axisymmetric solution Sol_0 to the set of multimoment hydrodynamics equations satisfactorily reproduces the steady flow $\mathbf{U}_0^{exp}(\mathbf{x})$ around the sphere. Upon reaching Re_0^*, the solution Sol_0 loses stability. The first unstable flow $\mathbf{V}_0^{exp}(t,\mathbf{x})$ around the sphere is satisfactorily described by the unstable axisymmetric solution Sol_0. Upon reaching Re_0^{**}, the solution Sol_0 for the periphery of the recirculating zone and in the far wake is replaced by the solution Sol_2, which describes a vortex ring moving downstream. The reason for the replacement is that the combination of solutions Sol_0 and Sol_2 provides a sharper drop in the entropy in the course of evolution than the solution Sol_0 does [16,17]. The combination of the solutions Sol_0 and Sol_2 describes the vortex shedding mode $\mathbf{W}_0^{exp}(t,\mathbf{x})$. At $\mathrm{Re} > \mathrm{Re}_0^{***}$, the solution Sol_2 at the periphery of the recirculating zone and in the far wake behind the sphere is replaced by the solution Sol_1, which also describes a vortex ring moving downstream. The reason for the replacement is that the combination of solutions Sol_0 and Sol_1 provides a sharper decrease in the entropy in the course of evolution than the combination of the solutions Sol_0 and Sol_2 does [16,17]. The combination of the solutions Sol_0 and Sol_1 describes the vortex sheet $\mathbf{Q}_0^{exp}(t,\mathbf{x})$.

The multimoment hydrodynamics confirms the ideas of experiment on unstable nature of the phenomenon of vortex shedding. The crossing of the first critical Reynolds number value Re_0^* is accompanied by the stability loss. The system loses its stability when entropy produced in the system can not compensate entropy outflow through the surface confining the system. Such interpretation follows directly from the principle of retention and loss of the open system stability formulated in Section 2. In accordance with solutions to the multimoment hydrodynamics equations, the system, when loses its stability, remains further unstable. One unstable flow is replaced by another unstable flow as Re grows. The replacement of one unstable regime by another is governed the tendency of the system to discover the fastest path to depart from the state of statistical equilibrium. This striving follows directly from the evolution criterion formulated in Section 2.

Since the time of L.Boltzmann, the responsibility for directing the evolution of the system rests with the initial conditions realized in the system, namely the set of initial values of the coordinates and velocities of all particles. For a given mutual arrangement of the particles, the system evolves in the direction that we see everywhere and every second. However, there are such arrangements of particles that direct the system in an extremely unlikely, rarely realized direction.

The pair entropy corresponding to the direct equations for pair distribution functions and the multimoment hydrodynamics equations they lead (2.2) can only be produced in the system due to binary collisions at each time point, $\Delta_{\mathrm{IN}} S_p(t) \geq 0$ [13]. Such behavior of the entropy is in full accordance with the second law of thermodynamics [6]. The solutions to the direct multimoment hydrodynamics equations describe the direction of evolution of the system that is everywhere and every second is found in nature. The pair entropy corresponding to the reverse equations for the pair distribution functions and the reverse multimoment hydrodynamics equations they yield (2.3) can only be absorbed in the system due to binary collisions at each time point, $\Delta_{\mathrm{IN}} S_p^{*(\alpha)}(t^*) \leq 0$. The solutions to the reverse multimoment hydrodynamics equations describe the evolution of the system in the opposite direction, which, as is commonly believed, is extremely rare in nature. The direct multimoment hydrodynamics equations are valid for the progressive direction of timing on the time axis pointing from the past to the future. The reverse multimoment hydrodynamics equations are valid for the progressive direction of timing on the time axis pointing from the future to the past. [8,14].

In [8,14], we failed to derive the reverse set of equations for pair distribution functions, which evolve with regressive direction of timing along the time axis pointing from the past to the future. As a consequence, we failed to rewrite the set of reverse multimoment hydrodynamics equations (2.3) and the reverse equation of entropy conservation (2.12) for regressive direction of timing along the time axis pointing from the past to the future. However, solutions to the reverse equations (2.3) and (2.12) are applicable to interpret observed system evolution with regressive timing along the time axis pointing from the past to the future. In [16,17] we used the same notation both for progressive timing on the time axis pointing from the future to the past and for regressive timing on the time axis pointing from the past to the future. This imprecision makes it difficult to understand the interpretation [16,17] of the calculation results. Relationships (3.1-3.4) help to resolve these difficulties.

At one time, L.Boltzmann, defending his point of view in disputes with opponents, suggested that exclusive conditions that guide the system in a highly unlikely direction arise very rarely. Apparently, Boltzmann's assumption is correct for a weak deviation of the system state from the state of statistical equilibrium. However, after crossing the border of the instability field, exclusive conditions arise with periodic regularity. This regularity manifests itself in each of the three unstable solutions that reproduce the flows $\mathbf{V}_0^{exp}(t,\mathbf{x})$, $\mathbf{W}_0^{exp}(t,\mathbf{x})$, and $\mathbf{Q}_0^{exp}(t,\mathbf{x})$.

The tendency of an unstable physical system to find the fastest way to recede from the state of statistical equilibrium does not lead the system to disintegration. At the time $t = t_*$, the entropy stops decreasing. The multimoment

hydrodynamics equations are unable to provide solutions that would continue to divert the system from the state of statistical equilibrium. At the time $t = t_*$, solution to the multimoment hydrodynamics equations is replaced by solution to the reverse multimoment hydrodynamics equations. Reverse solution changes the direction of evolution and guides the system to the state of statistical equilibrium. Time intervals during which the system moves away from the state of statistical equilibrium are periodically followed by intervals within which the system tends to equilibrium. It is this periodicity that permits to interpret vortex shedding, a graphic example of periodic unstable phenomena.

References

1. Lebed IV, Umanskii SY. The Appearance and Development of Turbulence in a Flow Past a Sphere: Problems and the Existing Approaches to Their Solution. RJ Physical Chemistry B 2007;1: 52-73.

2. Lebed IV. About the Prospects for Passage to Instability. Open Journal of Fluid Dynamics 2013; 3: 214-229.

3. Schuster HG. Deterministic Chaos. Weinheim: Physik_Verlag; 1984.

4. Johnson TA, Patel VS. Flow Past a Sphere Up to a Reynolds Number of 300. Journal of Fluid Mechanics 1999: 378; 19-70.

5. Loitsyanskii LG. Mechanics of Liquids and Gases. Oxford: Pergamon; 1966.

6. Liboff RL. Introduction to the theory of kinetic equations. New York –London–Sydney–Toronto: Willey; 1969.

7. Lebed IV, Method of Two-Particle Distribution Functions. Hydrodynamic Equations. Chemical Physics Reports 1996; 15: 861-883.

8. Lebed IV. Hydrodynamic Equations Stemming from Two Particle Distributions in the Limit of Weak Non- equilibrium. Analysis of Invertibility of Equations. Chemical Physics Reports 1996; 15: 1725- 1750.

9. Lebed IV. Derivation of the Equations for Pair Distribution Functions. Chem. Phys. Reports 1995; 14: 599-615.

10. Lebed IV. Equations of Pair Distribution Functions. Chem. Phys. Letters 1990; 165: 226-228.

11. Lebed IV. Kinetic Foundation for the Multimoment Hydrodynamics Equations. Open Journal of Fluid Dynamics 2015; 5: 76-91.

12. Lebed IV. The Method of Pair Functions as Applied to the Problem of a Flow around a Quiescent Solid Sphere. Chemical Physics Reports 1997; 16: 1263- 1301.

13. Lebed IV. About the Behavior of the Entropy of a Gas Flow Losing Its Stability. Chemical Physics Reports 1998; 17: 411-439.

14. Lebed IV. About Appearance of the Irreversibility. Open Journal of Fluid Dynamics 2014; 4: 298-320.

15. Lifshitz EM, Pitaevskii LP. Course of Theoretical Physics,Vol. 9: Statistical Physics, Part 2. New York: Pergamon; 1980.

16. Lebed IV. Multimoment Hydrodynamics in Problem on Flow around a Sphere: Entropy Interpretation of the Appearance and Development of Instability. Open Journal of Fluid Dynamics 2014; 4: 163-206.

17. Lebed IV. Development of Instability in the Problem of Flow around a Sphere. RJ Physical Chemistry B 2014; 8: 240-253.

ISSN 2347-3487

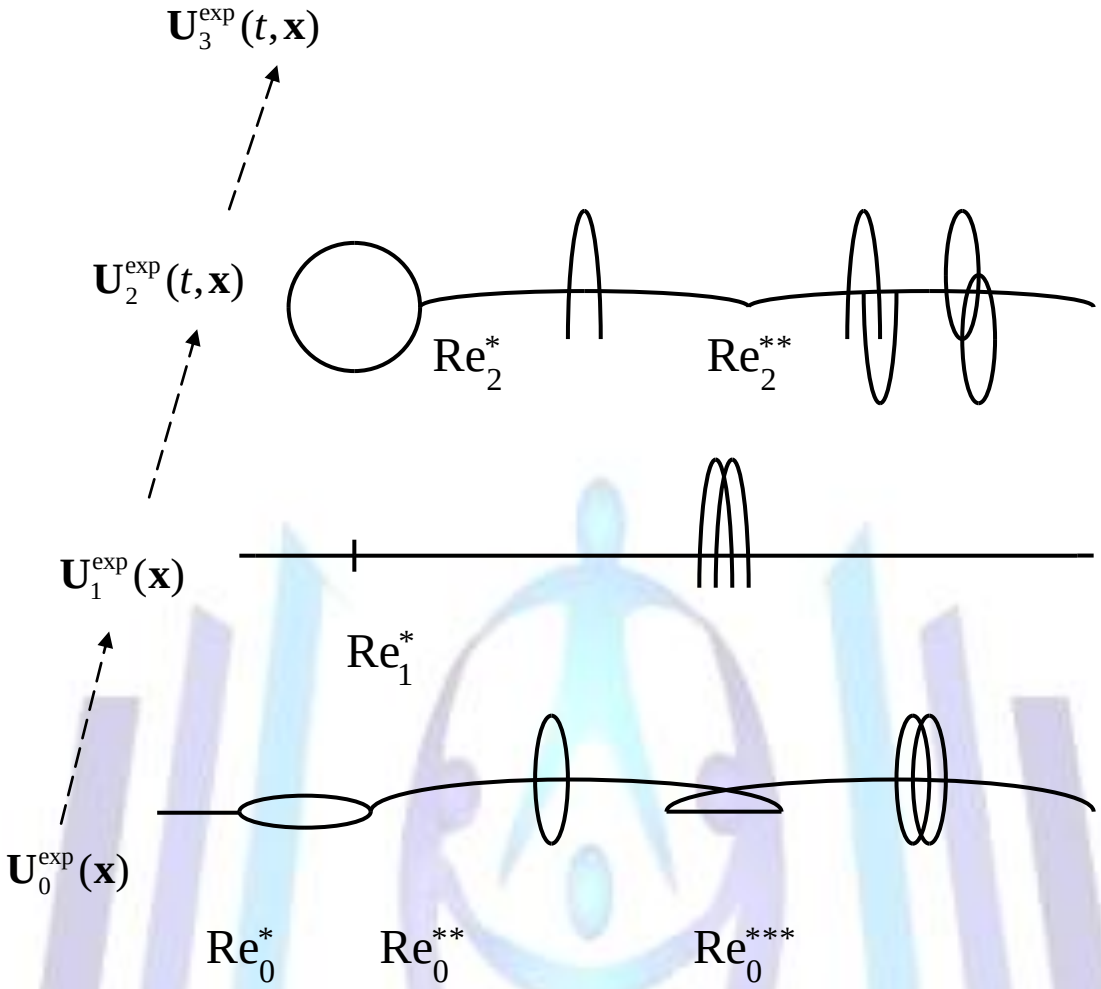

Figure 1. Three stable medium states originating three turbulence development directions for flow past a sphere. The lower branch corresponds to the evolution of ground stationary axisymmetric flow $\mathbf{U}_0^{exp}(\mathbf{x})$: $\mathrm{Re} < \mathrm{Re}_0^* - \mathbf{U}_0^{exp}(\mathbf{x})$; $\mathrm{Re}_0^* < \mathrm{Re} < \mathrm{Re}_0^{**}$, periodic pulsations of the axisymmetric recirculating zone in the wake behind a sphere $\mathbf{V}_0^{exp}(t,\mathbf{x})$; $\mathrm{Re}_0^{**} < \mathrm{Re} < \mathrm{Re}_0^{***}$, vortex ring shedding along a spiral path $\mathbf{W}_0^{exp}(t,\mathbf{x})$; and $\mathrm{Re} > \mathrm{Re}_0^{***}$, helicoidal vortex sheet $\mathbf{Q}_0^{exp}(t,\mathbf{x})$. The middle branch corresponds to the evolution of stable steady non-axisymmetric flow $\mathbf{U}_1^{exp}(\mathbf{x})$: $\mathrm{Re}_1 < \mathrm{Re} < \mathrm{Re}_1^* - \mathbf{U}_1^{exp}(\mathbf{x})$; $\mathrm{Re} > \mathrm{Re}_1^*$, periodic horseshoe-shaped vortex loop shedding along a rectilinear path $\mathbf{V}_1^{exp}(t,\mathbf{x})$. The upper branch corresponds to the evolution of a stable central-type state $\mathbf{U}_2^{exp}(t,\mathbf{x})$: $\mathrm{Re}_2 < \mathrm{Re} < \mathrm{Re}_2^* - \mathbf{U}_2^{exp}(t,\mathbf{x})$; $\mathrm{Re}_2^* < \mathrm{Re} < \mathrm{Re}_2^{**}$, periodic horseshoe-shaped vortex loop shedding along one of the double undulated thread branches $\mathbf{V}_2^{exp}(t,\mathbf{x})$; and $\mathrm{Re} > \mathrm{Re}_2^{**}$, periodic vortex loop shedding along both double undulated thread branches $\mathbf{W}_2^{exp}(t,\mathbf{x})$, or periodic vortex ring shedding $\mathbf{Q}_2^{exp}(t,\mathbf{x})$.

ISSN 2347-3487

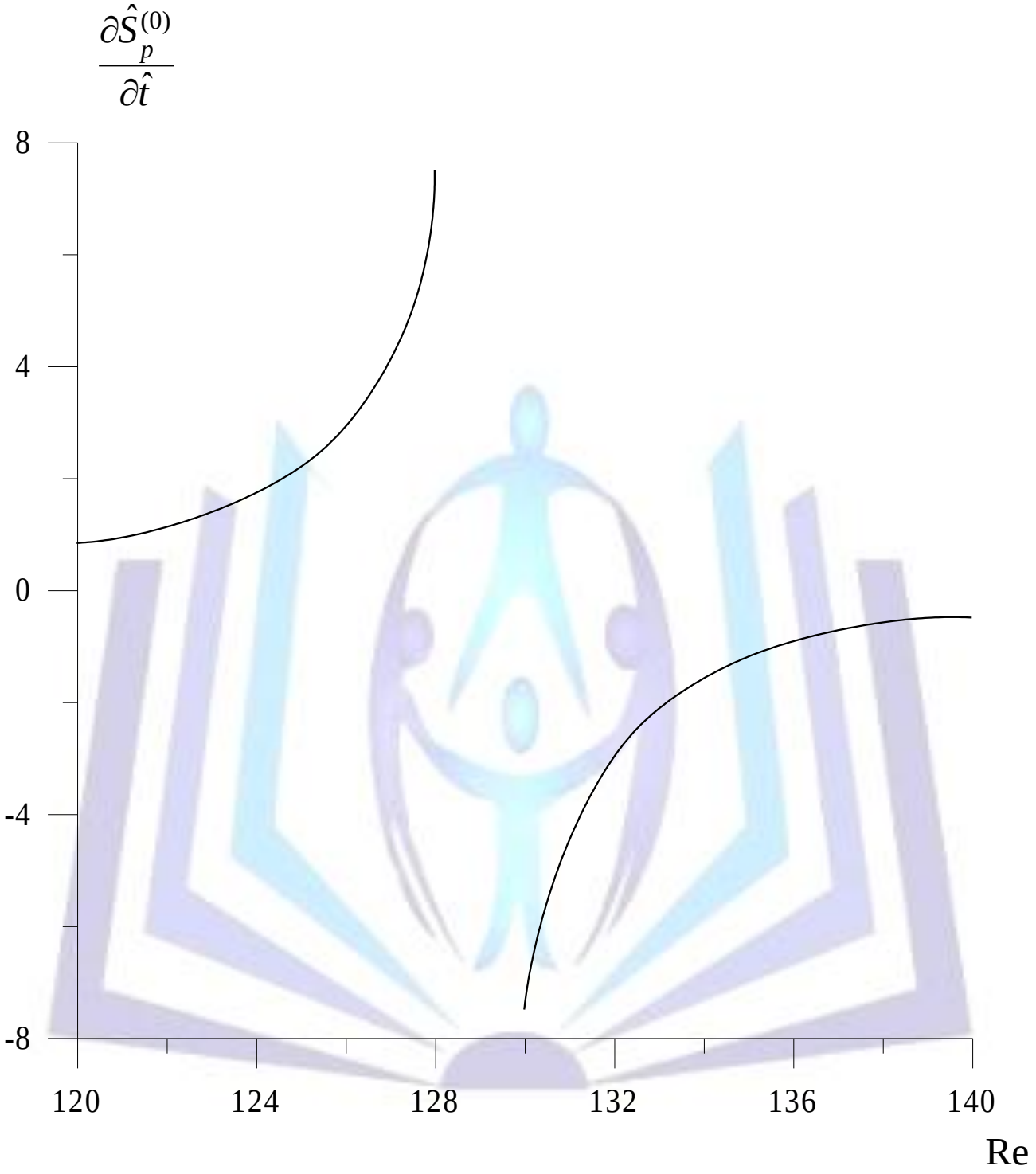

Figure 2. Pair entropy derivative $\partial \hat{S}_p^{(0)} / \partial \hat{t} = \partial \delta \hat{S}_p^{(0)} / \partial \hat{t}$ **as a function of Re,** $\mathrm{Re}_0^* = 129.1$**. The curves correspond to** $(\partial \delta \hat{S}_p^{(0)}(t) / \partial \hat{t}) \cdot 10^4$**.**

ISSN 2347-3487

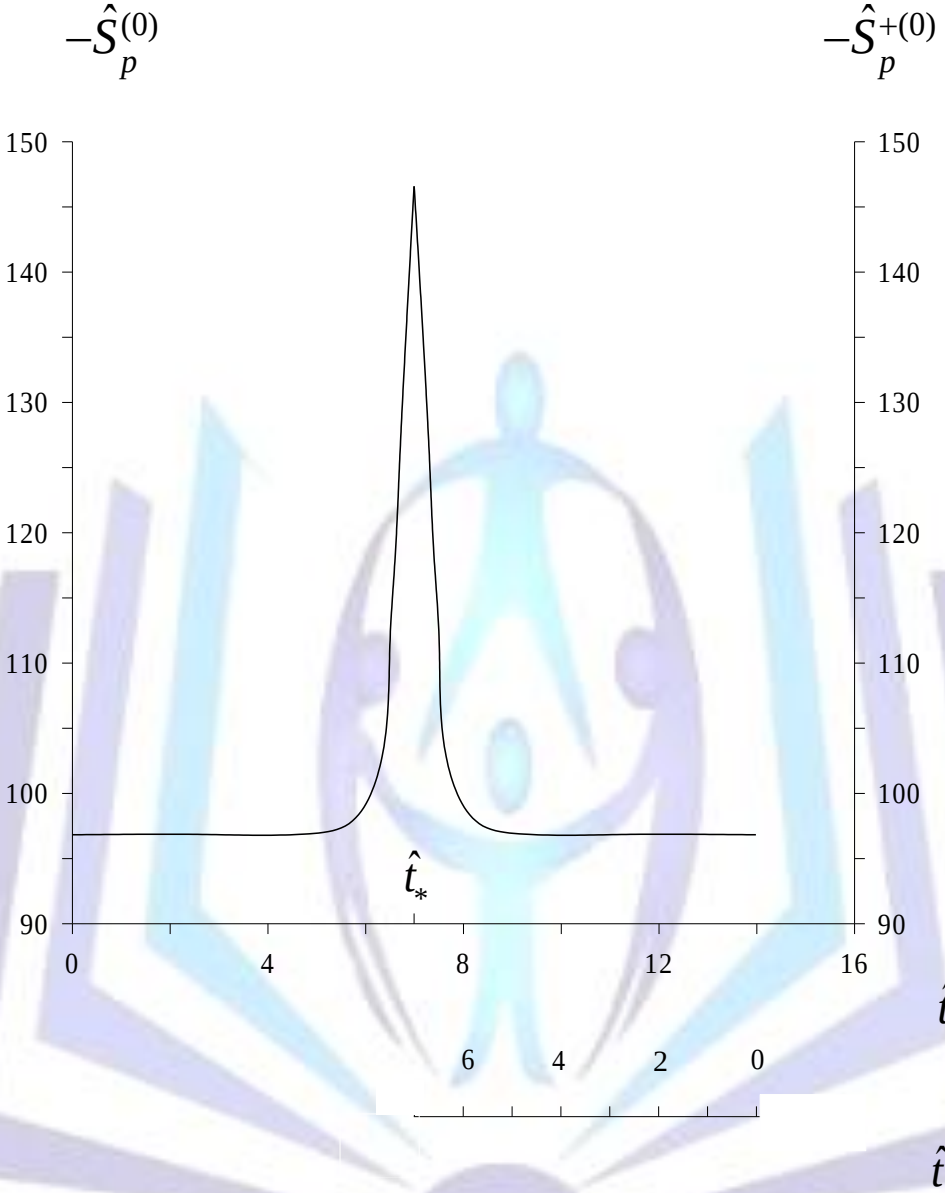

Figure 3. Time behavior of the pair entropy $\hat{S}_p^{(0)}(t)$, $\hat{S}_p^{+(0)}(t^+)$, Re = 400, $\hat{t}_*$ = 6.99.

ISSN 2347-3487

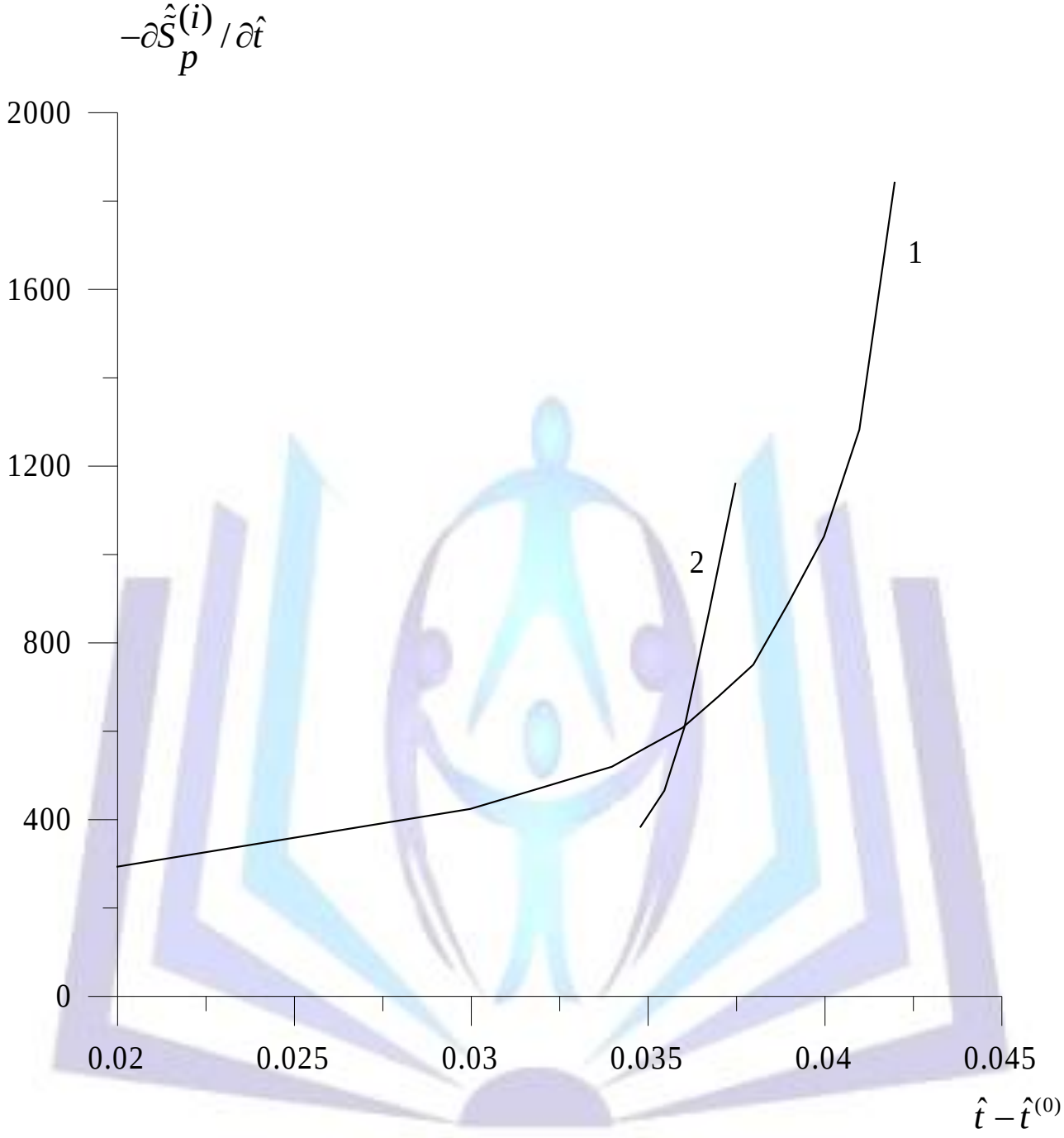

Figure 4. Time dependence of the entropy derivative $\partial\hat{\tilde{S}}_p^{(i)}(t - t^{(0)})/\partial\hat{t}$, $i = 0,1$. **The** $\partial\hat{\tilde{S}}_p^{(0)}(t - t^{(0)})/\partial\hat{t}$ **function is represented by curve 1. The** $\partial\hat{\tilde{S}}_p^{(1)}(t - t^{(0)})/\partial\hat{t}$ **function is represented by curve 2, Re = 400,** $\hat{t}^{(0)}$ **= 6.95. The time of restructuring is** $\hat{t}_1 = \hat{t}^{(0)}$ **+ 0.036.**